The Low Rate Telemetry Transmission Simulator

Jiří ŠPAČEK, Miroslav KASAL

Dept. of Radio Electronics, Brno University of Technology, Purkyňova 118, 612 00 Brno, Czech Republic

xspace07@stud.feec.vutbr.cz, kasal@feec.vutbr.cz

Abstract. *The presented paper is dedicated to the low rate telemetry transmission simulator. The basic concept of the system uses the carrier (DSB) and subcarrier (BPSK). The research is focused on the AWGN and carrier phase noise influence. Presented system can be extended with the described carrier phase noise model. In this paper, some issues related to the described model are also discussed. For example, the relation between bit error rate for uncoded bit stream and bit stream with differential coding, which is used in the model. Authors prove the using of Costas loops for very low energy per bit to noise power spectral density ratio. The influence of additive white Gaussian noise and phase noise is also investigated.*

Keywords

Low rate telemetry, Simulink® model, BPSK/DSB modulation, phase noise model, noise effect.

1. Introduction

Reception of very weak radio signals is done with very complex systems. The crux of the sensitivity in the modern systems is in very sophisticated post-processing. Nevertheless, the signal must be received with the "classical" receiver before post-processing is done. This receiver often utilizes Costas loops for carrier regeneration or for the demodulation. Costas loops are commonly used for signals with energy per bit to noise power spectral density ratio (E_b/N_o) bigger than 3 dB. Our research is partly focused on the behavior of Costas loops for E_b/N_o values lower than 3 dB and we also investigate the influence of the phase noise on Costas loops reliability. Accurate classification methods for the described circumstances have not been found in the available literature.

2. Basic System Model

The development and the results of simulations for the communication system with the NRZ/BPSK/DSB modulation are described in this paper. The block diagram of the system is presented in Fig. 1. The model has been developed by reason of research of the phase noise and additive white Gaussian noise, AWGN, influence on Bit Error Ratio BER for modulation with a subcarrier.

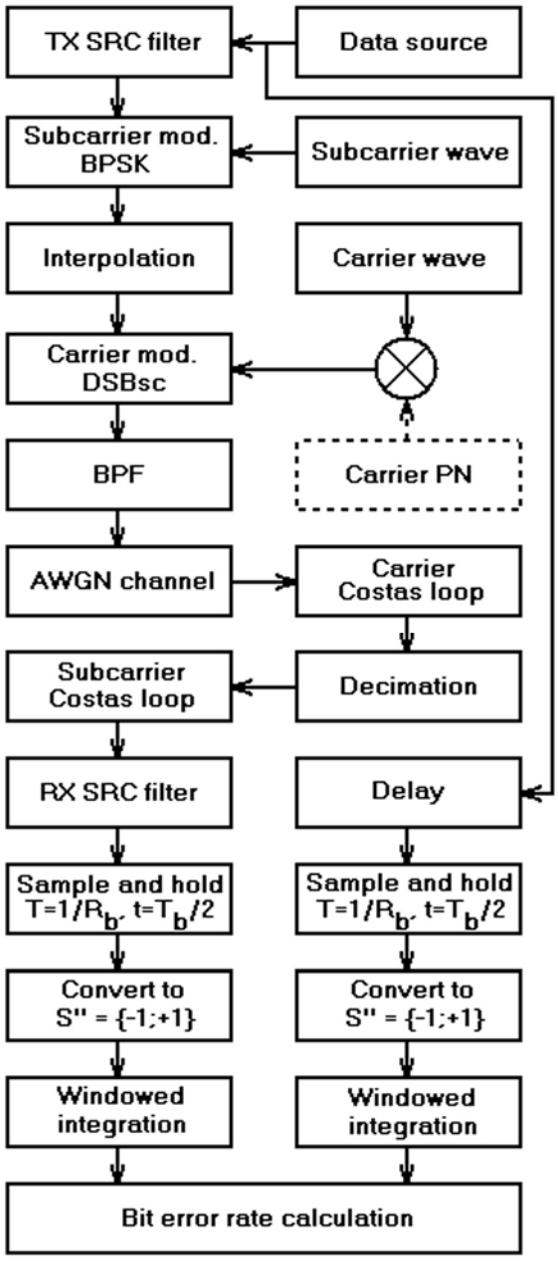

Fig. 1. The block diagram of the described communication system.

The subcarrier is used to shift the data signal from the carrier by reason of its effect reduction [1]. Regarding very low frequency of subcarrier, its own phase noise is negligible. Systems based on this principle are used in low rate telemetry link with very low energy per bit to noise power spectral density ratio E_b/N_o [2].

2.1 Baseband Data

As a *Data source*, the digital source with output set

$S = \{0 ; 1\}$

was used. Any of *Data source* states sequence can be chosen as presented in Tab. 1.

Option *A* in Tab. 1 presents the worst case with a single bit pulse duration $T_b = 1/R_b$, where R_b is bit ratio.

These $R_b = \{10, 50, 100, 500\}$ bps values have been used. Options *B* to *E* are used for the signal power determination after the following filtration with *Square root raised-cosine filter (SRC filter)* for given number of samples per bit N_{SRC} and modulation [3].

Option	Generator	Sequence
A	$Pulse_{1b}$	1010101010...
B	$Pulse_{2b}$	1100110011...
C	$Pulse_{3b}$	1110001110...
D	$Pulse_{4b}$	1111000011...
E	$Bernoulli_{p(0)=0}$	1111111111...
F	$Bernoulli_{p(0)=0.5}$	Random

Tab. 1. Data source output sequences.

The signal set for filtering with *SRC filter*, *S'*, is obtained with the simple substitution

$S = \{0 ; 1\} \Longrightarrow S' = \{-1 ; 1\}$.

Following this step, the baseband filtering was done. Parameters of the *SRC filter* were given as [4]: the roll-off factor $\alpha = 0.5$ and the number of samples per bit N_{SRC} was

$$N_{SRC} = \frac{f_{s\,SUB}}{R_b} \tag{1}$$

where $f_{s\ SUB}$ is the sampling frequency in baseband. This frequency was set on 128000 Hz in the presented work. Gain of the *SRC filter* is normalized, which means that the filter coefficients are normalized, too, so that the convolution of the filter with itself produces normal raised cosine filter whose peak coefficient equals to 1.

2.2 Subcarrier Modulation

The sine wave subcarrier [5] given as

$s_{sub} = \sin(2\pi f_{sub} t)$,

where f_{sub} is subcarrier frequency, BPSK is modulated by *SRC filtered* baseband signal. The value of subcarrier frequency in the presented work is $f_{sub} = 8$ kHz. The BPSK modulation is done with sample-by-sample multiplying.

After BPSK modulation, an interpolation $\{f_{s\ SUB} \Longrightarrow f_{s\ CARR}\}$ is used [6]. $f_{s\ CARR}$ is the sampling frequency in radio frequency band. Carrier frequency in the presented work is chosen $f_{carr} = 80$ kHz. Due to the request of minimum 8 samples/period, the new sampling frequency $f_{s\,CARR}$ and interpolation factor *I* are set as

$$f_{s\,CARR} \geq 8.f_{carr}\ ,\ I \geq \frac{f_{s\,CARR}}{f_{s\,SUB}} \tag{2 , 3}$$

where *I* must be an integer. Due to minimizing a computational time, we took the lowest possible value of the new sampling frequency and interpolation factor; $f_{s\,CARR} = 640$ kHz, $I = 5$.

Interpolation is done in standard way and uses zero samples inserted between all the following signal samples at $f_{s\ SUB}$. Subsequently, the signal is filtered with lowpass FIR filter [7]. This filter has the 30th order, passband gain *I* and cut-off frequency $f_c = 0.4 f_{s\ SUB}$.

2.3 Carrier Modulation

The sine wave carrier, given as

$s_{carr} = \sin(2\pi f_{carr} t)$,

where f_{carr} is carrier frequency, DSB is modulated by BPSK signal. The value of carrier frequency is $f_{carr} = 80$ kHz. The DSB modulation is done with sample-by-sample multiplying.

After the modulation, a band pass filter is used [4]. The purpose of this filter is removing the spurious spectral components after the DSB modulation. Filter cut-off frequencies are given as

$$f_{c\,low} = f_{carr} - f_{sub} - 2\ \text{kHz} = 70\ \text{kHz}\ , \tag{4}$$

$$f_{c\,high} = f_{carr} + f_{sub} + 2\ \text{kHz} = 90\ \text{kHz}\ . \tag{5}$$

Filter has the 18th order and it was designed with Chebyshev II (with ripple in stopband) approximation.

2.4 Additive White Gaussian Noise Channel

The NRZ/BPSK/DSB modulated signal then passes through the model of AWGN channel. Necessary AWGN channel parameters are input signal power P_{sig}, $\{E_b/N_o\}_{AWGN}$ and T_b.

Considering that power of a signal [8] is given as

$$P_{sig} = \lim_{T\to\infty} \frac{1}{T} \int_{-\frac{T}{2}}^{\frac{T}{2}} |f(t)|^2\, dt\ . \tag{6}$$

By this equation, it is possible to determine modulated signal power with (numerical) integration. Next [9], because the energy per bit E_b is given as

$$E_b = P_{sig}\, T_b \tag{7}$$

and the level of added noise in AWGN channel is specified by parameter $\{E_b/N_o\}_{AWGN}$, the spectral density of added noise N_o can be derived as

$$N_o = \frac{P_{sig} T_b}{10^{\frac{\{E_b/N_o\}_{AWGN}}{10}}} \,. \tag{8}$$

The values P_{sig} for signals used in described simulations are presented in Tab. 2. The values were obtained with numerical integration in Matlab®. In Tab. 2, the parameter *Filtered BS* describes if and how the data were filtered in baseband. The SRC filter was described in Section 2.1. The parameter *Filtered CA* determines if and how the signal was filtered after final modulation.

Data – filtered BS – modulation – filtered CA	Power [W]
Option A-F – no – BPSK – no	0.5
Option A – SRC – BPSK – no	$4.05.10^{-4}$
Option B – SRC – BPSK – no	$3.91.10^{-4}$
Option C – SRC – BPSK – no	$4.00.10^{-4}$
Option D – SRC – BPSK – no	$3.94.10^{-4}$
Option E – SRC – BPSK – no	$3.83.10^{-4}$
Option F – SRC – BPSK – no	$3.89.10^{-4}$
Option A – SRC – BPSK/DSB – no	$2.02.10^{-4}$
Option B – SRC – BPSK/DSB – no	$1.95.10^{-4}$
Option C – SRC – BPSK/DSB – no	$2.00.10^{-4}$
Option D – SRC – BPSK/DSB – no	$1.97.10^{-4}$
Option E – SRC – BPSK/DSB – no	$1.92.10^{-4}$
Option F – SRC – BPSK/DSB – no	$1.94.10^{-4}$
Option A – SRC – BPSK/DSB – Cheby	$2.02.10^{-4}$
Option B – SRC – BPSK/DSB – Cheby	$1.95.10^{-4}$
Option C – SRC – BPSK/DSB – Cheby	$1.99.10^{-4}$
Option D – SRC – BPSK/DSB – Cheby	$1.96.10^{-4}$
Option E – SRC – BPSK/DSB – Cheby	$1.91.10^{-4}$
Option F – SRC – BPSK/DSB – Cheby	$1.94.10^{-4}$

Tab. 2. Signal power P_{sig} for some data sequences, modulations and filtration, R_b = 100 bps.

2.5 Carrier Demodulation

After passing through the AWGN channel, the signal is demodulated with Costas loop [10]. The Costas loop performs DSB carrier demodulation. Because the data are modulated onto a sine wave subcarrier, the bandpass arm filters are used instead of lowpass. All bandpass arm filters are identical. Each of these filters has the 4th order and was designed with elliptic approximation and its cut-off frequencies are given as

$$f_{c\,low} = f_{sub} - 1\ \text{kHz} = 7\ \text{kHz}\,, \tag{9}$$

$$f_{c\,high} = f_{sub} + 1\ \text{kHz} = 9\ \text{kHz}\,. \tag{10}$$

The main loop filter is a lowpass. This filter has the first order, and it is designed with Chebyshev II (with ripple in stopband) approximation. The cut-off frequency of the main loop filter is

$$f_c \approx 3.(f_{c\,low} + f_{c\,high}) \approx 45\ \text{kHz} \tag{11}$$

where $f_{c\ low}$ and $f_{c\ high}$ are cut-off frequencies of bandpass arm filter.

The Costas loop uses a voltage controlled oscillator which has quiescent frequency f_o = 80 kHz and its gain was set to Gain_{VCO} = 10 Hz/V.

In the described Costas loop, the sampling frequency is $f_{s\,CARR}$. The decimation after the carrier demodulation is used.

Decimation $f_{s\ CARR}$ ==> $f_{s\ SUB}$ is done with lowpass filter followed by undersampling block [6]. Lowpass filter designed with elliptic approximation has the 7th order and its cut-off frequency is f_c = 40 kHz. After undersampling the new sampling frequency is $f_{s\,SUB}$ = 128 kHz.

2.6 Subcarrier Demodulation

Subcarrier demodulation is done by the Costas loop [11]. The loop uses two identical lowpass arm filters. Each of these filters has the 2nd order and its cut-off frequency [9] is given as

$$f_{ca} = f_b(1+\alpha) \tag{12}$$

where $f_b \equiv R_b$ and α is the roll-off factor of the used SRC filter. Lowpass arm filters are designed with Chebyshev I (with ripple in passband) approximation. Ripple of passband is up to 1 dB, nevertheless at frequency f_b ($\equiv R_b$) the attenuation is negligible.

The main loop filter has the 1st order, and it is designed with Chebyshev II (with ripple in stopband) approximation. The cut-off frequency of the main loop filter is

$$f_c \approx 2.f_{ca} \approx 300\ \text{Hz} \tag{13}$$

where f_{ca} is the cut-off frequency of the arm filter.

The Costas loop uses a voltage controlled oscillator which has quiescent frequency f_o = 8 kHz and its gain was set to Gain_{VCO} = 10 Hz/V.

2.7 Baseband Detection

After the demodulation, the *SRC filter* is used [3]. This filter presents the consecutive block to the *SRC filter* which is used in transmitter. Parameters of both these blocks are the same and they were described in Section 2.1.

SRC filtered data are sampled at rate of R_b with the time shift of $T_b/2$ and they are expressed as an element of the set

$$S'' = \{-1\ ;\ 1\}\,.$$

Next, the windowed integration over two samples (bits) is used. This approach is adequate to using the NRZI code [2], which is important for elimination the phase ambiguity of both Costas loops. The NRZI coding is also applied to transmitted data and results are compared for the Bit Error Rate calculation.

3. Phase Noise Model

We have a phase noise model which is able to model the user defined phase noise shape. The used model is partly based on the model for Matlab® by Alex Burr. The model is implemented in Simulink® as an Embedded Matlab function [12]. Inputs of the phase noise function are the sampling frequency f_s, the current simulation time t_{curr} and the shape of phase noise defined as two vectors; offset frequencies and phase noise level [dBc/Hz].

Phase noise is generated with inverse fast Fourier transformation IFFT as $N = f_s/10$ samples in agreement with the desired noise spectrum shape. The process of generation is periodical with the period of 0.1 sec. The implementation into real time simulation is done with the buffer length N and only one position in this buffer is read with the period $1/f_s$. Samples of phase noise are stored in the buffer.

The user defined phase noise spectrum shape is resampled to $N/2+1$ samples and it is smoothed with the division of log functions. Next, the spectrum shape is recalculated from dBc to relative value. Noise power for the n-th sample of spectrum is then marked as $P_{noise}(n)$.

Then, the $N/2+1$ samples of the normalized power ($P = 1$ W, $Z = 1\ \Omega$) of white Gaussian noise are generated. It can be written as

$$AWGN_{\text{norm}}(n) = \sqrt{Z\frac{P}{2}}.(\text{rand}(n) + ... \\ ... + j.\text{rand}(n)), \tag{14}$$

where power P is divided by 2 because of flipping the half of spectrum [8], which will follow next. The half of phase noise spectrum is then given as

$$X_{1/2}(n) = K.\sqrt{P_{\text{noise}}(n).d}.AWGN_{\text{norm}}(n) \tag{15}$$

where K is the IFFT normalizing coefficient and d is the normalizing coefficient of phase noise power.

The IFFT normalizing constant represents the determination of the phase noise appropriate power level with regards to the inverse Fourier transform process [3], which will be used next. The constant $1/K$ is presented in the inverse K-points Fourier transform definition

$$x(n) = \frac{1}{K}\sum_{k=1}^{K} X(k)\exp(j2\pi...) \tag{16}$$

and it has to be compensated with the multiplying $X(k)$ by the constant $K = N$.

The normalizing coefficient d conditions the power of phase noise according to the number of phase noise spectrum samples. It can be derived that its value is $d = N$.

Now, the full phase noise spectrum is calculated. The negative part of spectrum is given as the positive part conjugated and flipped over the point $f_s/2$ [6]. After flipping, the IFFT is applied, thus

$$x = IFFT\{X_{1/2}, X_{1/2}^*\} \tag{17}$$

and each sample of the phase noise is finally given as

$$PN(n) = \exp(j.\text{Re}\{x(n)\}). \tag{18}$$

Through the connection from Embedded Matlab® function to the Simulink®, the instantaneous variance of phase is sent for each sample. Finally [13], the carrier with phase noise is given as

$$s_{carr+PN}(n) = \cos(2\pi\frac{f_{carr}}{f_s}n + ... \\ ... + \text{Phase}\{PN(n)\}). \tag{19}$$

4. BER for Differentially Coded Signal

Our model uses Costas loops. The Costas loop has the 180 degrees phase ambiguity, which may cause the problem with detection of bit logical states [14]. To correct this problem, we implemented the NRZI differential decoder for subcarrier BPSK with windowed integrators in the model. This approach provides that each 180-degree change in the Costas loops causes only two errors in the received bit stream, but it also has the influence on the resulting bit error. This influence can be discussed as:

- the only one single error bit causes two errors after differential decoding,
- a burst with two or more error bits causes just two errors after differential decoding,
- obviously, the bit error rate for uncoded bit stream BER_1 has to be lower than the bit error rate for differentially coded bit stream BER_2.

For easy and transparent confrontation of the simulation results, we need to convert between both cases. The formula for conversion between BER_1 and BER_2 can be derived as follows. The theoretical formula for bit error rate of uncoded BPSK [8] is given as

$$BER_1 = 0.5\text{erfc}\left(\sqrt{E_b/N_o}\right), \tag{20}$$

while the BER of differentially coded BPSK [2] is given as

$$BER_2 = \text{erfc}\left(\sqrt{E_b/N_o}\right)... \\ ...\left(1 - \frac{\text{erfc}\left(\sqrt{E_b/N_o}\right)}{2}\right). \tag{21}$$

Using the substitution

$$A = \mathrm{erfc}\left(\sqrt{E_b / N_o}\right), \tag{22}$$

we can now derive the function $A = f(BER_2)$ with comparison of formulas (20) and (21). This function can be derived as

$$A^2 - 2A + 2BER_2 = 0. \tag{23}$$

The presented quadratic equation has two roots. As mentioned above, $BER_1 < BER_2$, thus

$$A = 1 - \sqrt{1 - 2BER_2} \tag{24}$$

and finally

$$BER_1 = \frac{1 - \sqrt{1 - 2BER_2}}{2}. \tag{25}$$

5. AWGN and Phase Noise Power

It is well known that the AWGN spectral density is constant along the frequency axis and its value was specified by relation (8) mentioned above. The power of AWGN in the limited bandwidth P_{AWGN} is then independent on an absolute position on the frequency axis [9] given as

$$P_{AWGN} = 10.\log(B_N.N_o) \tag{26}$$

where B_N is the noise bandwidth of the used filter. Its value [8] can be calculated as

$$B_N = \int_0^{\frac{f_s}{2}} \frac{H(f)}{\mathrm{Max}\{H(f)\}} df \tag{27}$$

where $H(f)$ is the magnitude response of the used filter.

The phase noise which is symmetrically dissociated around the centered carrier in the filter pass band [15] has the power

$$P_{PN\ symm} = 2\int_{\Delta f} L(f)df \tag{28}$$

where $L(f)$ is the one-sided phase noise absolute spectral density and Δf is given as $\Delta f = B_N$ for lowpass filter, and $\Delta f = B_N/2$ for bandpass filter, which is depicted in Fig. 2.

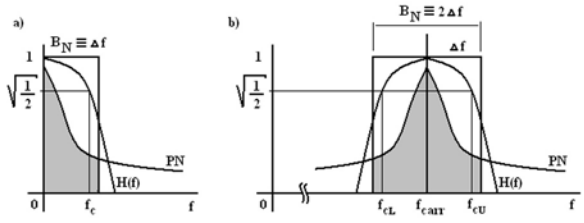

Fig. 2. Phase noise related to the lowpass filter pass band - **a),** Phase noise related to the bandpass filter pass band - **b).**

The mentioned approach is applicable only when the phase noise shape in the filter noise bandwidth is symmetrical. When we have a look at the effect of carrier phase noise on the modulated subcarrier, the situation is different. Here, the phase noise in the noise bandwidth is not symmetrical. The phase noise power for the nonsymmetrical dissociation of phase noise power $P_{PN\ non}$ over the filter bandwidth [16] can be calculated as

$$P_{PN\ non} = \int_{B_N} L(f)df \tag{29}$$

where $L(f)$ is the one-sided phase noise absolute spectral density and B_N is the noise bandwidth of the bandpass filter, as is depicted in Fig. 3.

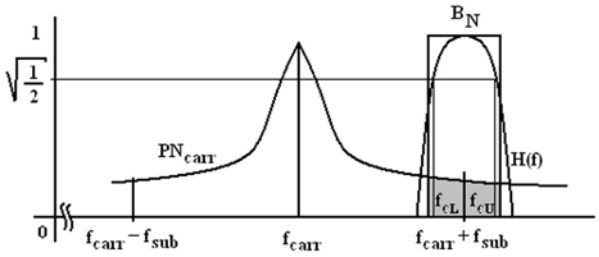

Fig. 3. The carrier phase noise related to the subcarrier bandpass filter pass band.

The single side phase noise shape in the described model is defined by a user as linear approximation in dBc/Hz over logarithmic frequency axis. The example of spectral approximation is presented in Fig. 4. The slope of the *n*-th approximation segment is C_n [dB/dec], the edge points are in frequencies $f_n = 10\text{^}n$, 10^^{n+1}, and the phase noise level in those points are PN_n. The filter noise bandwidth is bordered by the frequencies f_L and f_U.

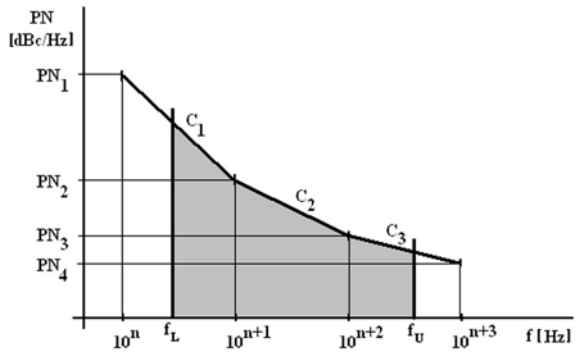

Fig. 4. The example of carrier phase noise approximation.

The integration has to be done over the smooth function. In the example case, the phase noise spectrum shape has to be divided to three integrable functions which will be presented by three abscisae in direction form [17]. Their equations are

$$y_i = \frac{C_i}{10^{n+i} - 10^{n+i-1}} x + q_i \tag{30}$$

where the variable y is related to the phase noise power, the variable x is related to the frequency and coefficients q_i are given as

$$q_i = PN_i - \frac{C_i}{10^{n+i} - 10^{n+i-1}} . 10^{n+i-1} \ . \tag{31}$$

In the example presented in Fig. 4, the relation (29) can be written out, and phase noise power in the noise bandwidth is then given as

$$P_{\text{PN nonsym}} = \int_{f_L}^{f_U} PN(f)df = \int_{f_L}^{10^{n+1}} 10^{y_1} dx + ... \\ ... + \int_{10^{n+1}}^{10^{n+2}} 10^{y_2} dx + \int_{10^{n+3}}^{f_U} 10^{y_3} dx \ . \tag{32}$$

For the narrow filter bandwidth, when both f_L and f_U are in the region with the same approximation abscissa (for example abscissa C_1 in Fig. 4), equation (29) can be written out as

$$P_{\text{PN nonsym}} = \int_{f_L}^{f_U} PN(f)df = \int_{f_L}^{f_U} 10^{y_1} dx \ . \tag{33}$$

6. Calibration and Results

The system described in section 2 had been implemented in the Matlab®-Simulink® environment. After the implementation, the system was calibrated. Calibration means that the setup of all system blocks is done in such way, that the model provides reliable results in the well known circumstances and this process is closely connected with the theory described above. The calibration is very complex and therefore it was divided into two steps.

First, only the subcarrier part of model (BPSK) was implemented and calibrated. The result of this calibration step is presented in Fig. 5.

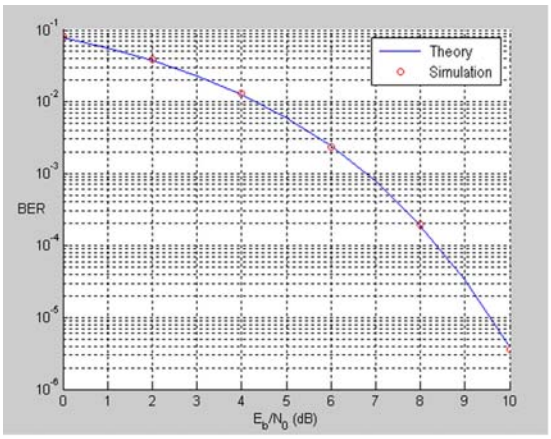

Fig. 5. The result of the first calibration step.

After the successful calibration of the subcarrier part, the model was extended with the carrier part (DSB) and the calibration process was done again. The result is presented in Fig. 6.

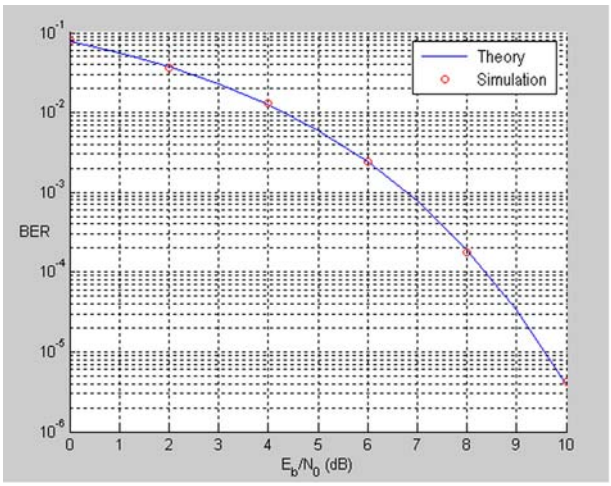

Fig. 6. The result of the second calibration step.

With the calibrated system, the AWGN influence was investigated. This work focuses on the improvement of noise conditions for the AWGN due to the use of Costas loops. For this purpose, the unmodulated signal with various level of additive white Gaussian noise was used. The power of this signal was calculated in the test points. Test points are defined in Fig. 7.

From the power of AWGN in the test point, the equivalent noise bandwidth of a fictive filter B_{Nf} can be calculated, which has to be used instead of the previous section of the receiver for obtaining the same noise power in the test point. The value B_{Nf} defined in this way is for points II and IV very close to the bandwidth of the contiguous Costas loop. When considering the results presented next, especially for points IV and V, it is obvious that the improvement of noise conditions due to Costas loops is essential.

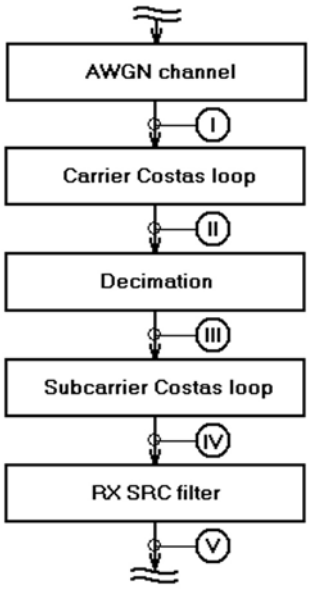

Fig. 7. The test points for the power calculation.

All of the following simulations were done with unmodulated signal. The parameters of all simulator blocks

were set correctly for the actual rate $R_b = \{10,50,100,500\}$ bps, using the values obtained by formulas described in Section 2. The simulation can be described as follows. Firstly, the power of signal without AWGN P_s in all test points was calculated. After that the power P_{s+n} of noisy signal with $E_b/N_o = \{0, 4, 8\}$ dB was calculated in all test points. The power of noise P_n in the actual test point for each case is then given as

$$P_n = P_{s+n} - P_s \ . \tag{34}$$

For the noise power P_n, the value of spectral noise density N_o can be calculated with relation (8). Finally, the equivalent noise bandwidth of the fictive filter B_{Nf} for the actual test point can be calculated from relation (26). The results are presented in Tab. 4.

Test point	R_b [bps]	E_b/N_o [dB]	B_{Nf} [Hz]
I	all	all	320000
II	all	0	1250.2
		4	1249.5
		8	1249.0
III	all	0	1023.2
		4	1022.3
		8	1021.9
IV	10	0	3.07
		4	2.80
		8	2.64
	50	0	15.8
		4	15.4
		8	14.6
	100	0	32.0
		4	31.5
		8	30.6
	500	0	164.0
		4	162.9
		8	161.0
V	10	0	0.68
		4	0.52
		8	0.36
	50	0	3.36
		4	3.03
		8	2.56
	100	0	6.54
		4	5.98
		8	5.07
	500	0	35.1
		4	34.0
		8	32.2

Tab. 4. The fictive noise bandwidth in selected points of the simulator for various rate and E_b/N_o.

The equivalent noise bandwidth B_{Nf} in the Test point I is equal to the $f_{s\,CARR}/2$ for all simulations. This result is in accordance with the hypothesis. Setting of the carrier Costas loop and decimation filter is the same for all tested rates $R_b = \{10,50,100,500\}$ bps. Small differences between values of B_{Nf} for various E_b/N_o in Test points II and III claim the fact that the improvement of noise conditions due to Costas loop is slightly deteriorating when the value of E_b/N_o decreases.

The setting of the subcarrier Costas loop and the RX SRC filter is dependent on the actual R_b. With results for the Test point IV, the coefficient of noise conditions improvement due to the addition of subcarrier Costas loop can be implied as

$$\left.\frac{f_{ca}}{B_{Nf}}\right|_{T.P.IV.} \approx 4.6 \div 5.7 \ .$$

As it is more specified in Fig. 8a, this coefficient depends on the values of E_b/N_o and R_b. Similarly, with results for the Test point V, the coefficient of noise condition improvement due to the addition of RX SRC filter can be implied as

$$\left.\frac{f_{ca}}{B_{Nf}}\right|_{T.P.V.} \approx 21 \div 42 \ .$$

As it is more specified in Fig. 8b, this coefficient also depends on the values of E_b/N_o and R_b. In Fig. 8, it is obvious that the effect of the value E_b/N_o is more perceptible for lower bit rates.

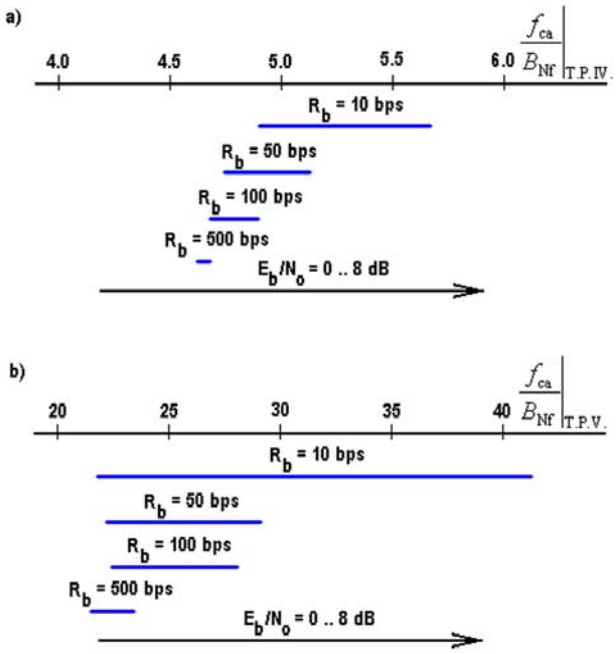

Fig. 8. **a)** The coefficient of noise conditions improvement in Test point IV, **b)** The coefficient of noise conditions improvement in Test point V.

7. Conclusion

Our work is focused on the research of additive white Gaussian noise and the phase noise influence on the reliability of the communication system with the coherent detection. We performed simulations of the low rate system, which uses the sine wave subcarrier. This approach is commonly used for the applications, where the value E_b/N_o is very low. The typical example is the space probes telemetry transmission.

Currently, we have a simulator, which is able to provide reliable results for the additive white Gaussian noise incidence. The next research will be focused on the phase noise effects.

Acknowledgements

The research is financially supported by the Czech Grant Agency under the doctoral project No. 102/03/H109 "Methods, Structures and Components of Electronic Wireless Communication" and the project No. 102/06/1672 "Communication Systems of Experimental Satellites".

References

[1] SHIHABI, M., SHAH, B., HINEDI, S., MILLION, S. Residual and suppressed carrier arraying techniques for deep-space communications. *TDA Progress Report*. 1995, vol. 121, 29 p.

[2] LINDSEY, W. C., SIMON, M. K. *Telecommunication Systems Engineering*. New York: Dover Publications, Inc., 1973.

[3] ŠEBESTA, V. *Theory of Telecommunication.* Lecture notes, Brno University of Technology, Brno, 2001. (In Czech.)

[4] MARTIN, W. L., NGUYEN, T. M. *CCSDS – SFCG Efficient Modulation Methods Study – A Comparison of Modulation Schemes – Phase 1: Bandwidth Utilization*. Recommendation for space data system standards, CCSDS B20.0-Y, 1993.

[5] KINMAN, P. W. *34-m and 70-m Telemetry Reception*. DSMS Telecommunications Link Design Handbook, 2003.

[6] KOZUMPLIK, J., KOLAR, R., JAN, J. *Digital Signal Processing and Analysis*. Lecture notes, Brno University of Technology, Brno, 2001. (In Czech.)

[7] *Proceedings of the CCSDS RF and Modulation Subpanel 1E on Bandwidth-Efficient Modulations*. Report concerning space data system standards, CCSDS B20.0-Y-2, 2001.

[8] ŽALUD, V. *Modern Radio Electronics*. Prague: BEN publishing, 2000. (In Czech.)

[9] KASAL, M. *Radio Rellay and Satellite Communication*. Lecture notes, Brno University of Technology, Brno, 2003. (In Czech.)

[10] VITERBI, A. J. *Principles of Coherent Communication*. Moscow: Sovetskoe radio, 1970. (In Russian.)

[11] STEVENS, G., WOO, K. T. Design of a Costas loop to operate with the Block III receiver and its predicted performance. *DSN Progress Report.* 1979, vol. 51, 11 p.

[12] *Communications Blockset for Use with Simulink®*. The MathWorks® Reference, The MathWorks Inc., 2004.

[13] KUNDERT, K. *Modeling and Simulation of Jitter in Phase-Locked Loops*. Cadence Design Systems, California, 2002.

[14] PAAL, L., SNIFFIN, R. W. *Telemetry Data Decoding*. DSMS Telecommunications Link Design Handbook, 2004.

[15] KASAL, M. *Frequency Synthesis in Communication Systems Experimental Satellites*. Brno: VUTIUM, Brno University of Technology, 2005. (In Czech.)

[16] ROBERTS, N. Phase noise and jitter – A primer for digital designers. *EE Design* (www.eedesign.com). 2003, 11 p.

[17] LOSTAK, J. *The Lexicon of Mathematics*. Olomouc: FIN publishing, 1996. (In Czech.)

[18] HACKE, L. J., WOOD, G. E. Laboratory and Flight Performance of the Mars Pathfinder (15, 1/6) Convolutionally Encoded Telemetry Link. *TDA Progress Report.* 1997, vol. 129, 11 p.

[19] *Telemetry Synchronization and Channel Coding*. Recommendation for space data system standards, CCSDS 131.0-B-1, 2003.

[20] KASAL, M. *Modern Methods of Generation and Signal Processing in Nuclear Magnetics Resonance*. Inaugural dissertation, Brno University of Technology, Brno, 1998. (In Czech.)

[21] *Bandwidth-Efficient Modulations – Summary of Definition, Implementation, and Performance*. Report concerning space data system standards, CCSDS 413.0-G-1, 2003.

[22] *Radio Frequency and Modulation Systems*. Recommendation for space data system standards, CCSDS 401.0, 2005.

[23] LAM, L., MILLION, S. Performance of pulse code modulation / phase modulation receivers with nonideal data. *TDA Progress Report.* 1997, vol. 128, 17 p.

[24] *Telemetry – Summary of Concept and Rationale*. Report concerning space data system standards, CCSDS 100.0-G-1, 1987.

[25] STEBER, J. M. *PSK Demodulation*. TechNote, San Jose: WJ Communications, Inc. 2001.

[26] SUE, M. K. Block IV receiver tracking loop performance in the presence of a CW RFI. *TDA Progress Report.* 1980, vol. 60, 13 p.

[27] HURD, W. J., MILEANT A. Improved carrier tracking for low-threshold telemetry using a smoother. *TMO Progress Report.* 2000, vol. 141, 16 p.

[28] NOREEN, G. K. *Deep Space Network Support of Small Missions*. Jet Propulsion Laboratory, California Institute of Technology, California, 2003.

[29] HAGHIGHAT, A. *Low-Jitter Symbol Timing Recovery for M-ary QAM and PAM Signals*. A thesis in the Department of Electrical Engineering, Concordia University, Canada, 1998.

[30] WARREN, L. M. *DSN Support of Earth Orbiting and Deep Space Missions*. Jet Propulsion Laboratory, California Institute of Technology, California, 1994.

[31] KUIPER, T. B. H., RESCH, G. M. *Deep Space Telecommunications*, Jet Propulsion Labolatory, California Institute of Technology, California, 2001.

[32] CHI, X. *DSP Implementation of Communication Systems - Carrier recovery using a second order Costas loop*. Lecture note, Virginia Polytechnic Institute and State University, Virginia, 2002.

[33] KARSI, M. F., LINDSEY, W. C. Effects of CW interference on phase-locked loop performance. *IEEE Transactions on Communications.* 2000, vol. 48, no. 5.

[34] AKINLI, C., GAMACHE, M., ROSE, M., ROST, A., SALES, J. TANG, J. Telemetry, tracking, communications, command and data handling. *TMO Progress Report.*2001, vol. 145, 77 p.

[35] CHEN, C. C., SHAMBAYATI, S., MAKOVSKY, A., TAYLOR, F. H., HERMAN M. I., ZINGALES, S. H. *Small Deep Space Transponder (SDST) – Technology Validation Report*. JET Propulsion Lab., California Inst. of Technology, California, 2000.

About Authors...

Jiří ŠPAČEK was born in Zlín, Czech Republic, in 1981. He received his master's degree in electrical engineering from the Brno University of Technology in 2002. At present, he is a PhD student at the Department of Radio Electronics, Brno University of Technology. His research interest is focused on the technology for the extremely weak deep space probes signals reception.

Miroslav KASAL (born in 1947 in Litomyšl, Czech Republic) graduated in communication engineering from the Faculty of Electrical Engineering, Brno University of Technology, in 1970. In 1984 he obtained his PhD degree in metering engineering. He was the head of the NMR Department and Electronics Laboratory of the Institute of Scientific Instruments, Academy of Science of the Czech Republic (1991 – 2002). Since 2002 he has been with the Department of Radio Engineering, Faculty of Electrical Engineering and Communication, Brno University of Technology, as professor. Dr. Kasal is a senior member of the IEEE. He has authored or coauthored a number of papers in scientific journals and conference proceedings. In 2004 he received the Award of the Rector of the Brno University of Technology and the SIEMENS Prize for research.